Investigation of the Macroscopic Characteristics of Hydrotreated Vegetable Oil (HVO) Spray using CFD method

Zhichao Zhang [a,b], Yiji Lu [a,b,*], Anthony Paul Roskilly [a,b], Xiaoli Yu [b], Yaodong Wang [b], Andrew Smallbone [b]

[a] *Department of Energy Engineering, Zhejiang University, Hangzhou 310027, China*

[b] *Sir Joseph Swan Centre for Energy Research, Newcastle University, Newcastle NE1 7RU, United Kingdom*

Abstract

The main macroscopic characteristics of Hydrotreated Vegetable Oil (HVO) spray in both injection and post-injection periods are investigated via Computational Fluid Dynamics (CFD) in this research. A 2D CFD work employing the Wave breakup model and KHRT breakup model are validated by the experimental data from a Constant Volume Vessel (CVV). Spray tip penetration and cone angle are obtained by the CFD model under various conditions, where the rail pressure, fuel temperature, ambient pressure and ambient temperature are independently varying. Results demonstrate that the Wave model has overall higher precision in predicting the spray tip penetration and the average cone angle than the KHRT model. By the End of Injection (EOI), spray tip penetration is significantly increased by increasing rail pressure and decreasing ambient pressure. While the average cone angle is larger at high ambient pressure but not sensitive to rail pressure at the cold ambient condition. The average cone angle during injection can be enlarged by high

* Corresponding author. Tel.: +44 (0) 191 208 4827
E-mail address: yiji.lu@ncl.ac.uk; luyiji0620@gmail.com (Y. Lu)

ambient temperature, especially when the rail pressure is also high. Nevertheless, spray tip penetration can only be slightly promoted by high ambient temperature. Fuel temperature has no comparable impact on spray tip penetration and cone angle during injection. In the post-injection period (after the EOI), ambient temperature becomes dominant and spray tip penetration can be reduced by either ambient temperature or fuel temperature. An empirical model is also correlated via Design of Experiments (DoE) and has high precision in predicting spray tip penetration after the breakup time.

***Keywords**:* Biodiesel; Spray performance; Computational fluid dynamics (CFD); Constant volume vessel; Design of experiments (DoE);

1. Introduction

Biodiesel produced by transesterification, usually refer to fatty acid methyl esters (FAME). The unsaturated compositions of FAME have adverse influence on the oxidation stability leading to the limitation on their percentage blending with standard diesel fuel [1]. As a second-generation biodiesel, Hydrotreated Vegetable Oil (HVO) is the mixture of n- and i-paraffin, which are the products of hydrogenation. Compared with biodiesels, HVO has high cetane number and high energy density, and excludes aromatics, naphthene, sulphur and oxygenates, which enables high oxidation stability and high percentage of blending with standard diesel fuel [1, 2]. As a result, it is beneficial in improving engine output and reducing emissions. Furthermore, unlike biodiesels, HVO has good storage stability and excellent cold starting without suffering from deposition and low engine output, and thus makes it a superior alternative fuel [3, 4].

Previously reported research on HVO mainly focus on its performance in engines or vehicles [5]. For example, Millo et al. [1] studied the emissions of HVO and some other biofuels in a diesel engine and found reduced CO and unburnt hydrocarbons (UHC) but comparable NO_x emissions

with standard diesel fuel. Sugiyama et al. [6] did similar research on HVO in an inline 4 cylinder diesel engine at fixed speed and varying torque and found soot can also been reduced apart from CO and UHC, but NO_x emissions sometimes were higher than standard diesel fuel. Lehto et al. [7] studied HVO in a single-cylinder engine with 30% exhaust gas recirculation (EGR) and demonstrated HVO generated less smoke and can adapt to higher EGR conditions than standard diesel fuel. Singh et al. [8] employed a heavy-duty diesel engine to study the emissions and fuel consumption of HVO. It was reported that the particulate matter (PM), carbon monoxide (CO), unburnt hydrocarbon (UHC) and brake specific fuel consumption (BSFC) were all lower than those of diesel fuel. However, most researches of HVO were about its engine performance, but its spray characteristics were rarely mentioned.

The spray is an important process for liquid fuels, as it influences the performance of in-cylinder combustion and thus determines the formation of pollutants. A series of studies of various fuels were conducted on the spray characteristics. Chen et al. [9] compared the spray properties of biodiesel and its blend with standard diesel and found biodiesel experienced longer penetration and larger size of droplets. Nevertheless, this study was done at room temperature and room pressure, which is far from the condition in the diesel engine. Mohan et al. [10] demonstrated that spray penetration reduces with increasing ambient pressure, while Gao et al. [11] found it increases almost linearly with increasing injection pressure at the initial breakup stage. However, these studies did not consider the effect of ambient temperature. In contrast, several researchers [12-14] investigated various fuels spray at a different ambient temperature and all reported reduced penetration at high ambient temperature. On one hand, the ambient pressures in these studies were all not set to constant when increasing the ambient temperature, so the reduced penetration cannot be certainly attributed to increasing ambient temperature. On the other hand, the previously

reported works were all about esterified biofuels or alcohol substances but not HVO. Hulkkonen et al. [15] and Sugiyama et al. [6] compared the spray properties of HVO and standard diesel fuel at the same conditions but found no significant difference between them in terms of spray tip penetration and cone angle. In contrast, Thomas et al. [16] investigated the spray characteristics of some biofuels containing HVO at constant ambient temperature and pressure and reported HVO produced the shortest spray tip penetration and the largest overall cone angle. However, the influences of injection pressure, fuel temperature, ambient pressure and ambient temperature were not considered in the work.

Numerical studies were also conducted on liquid fuel spray by computational fluid dynamics (CFD) simulation. The Wave breakup model [17] and KHRT breakup model [18] were the two widely used breakup models for spray in the CFD simulation, and the results of the models showed a good agreement with experimental data when predicting spray characteristics of various fuels in previous researches [19-22]. However, none of these researches covered all the effects of injection pressure, fuel temperature, ambient temperature and ambient pressure, and HVO was also not mentioned in these numerical works. Gong et al. [23] built CFD models for HVO spray via the large eddy simulation (LES) and RANS respectively. The models were run at both non-evaporating and evaporating conditions and their results on liquid and vapour penetrations as well as the Sauter Mean Diameter (SMD) agree with experimental data well. However, only the impact of ambient temperature was analysed in the models. The differences in droplet size and spray tip penetration between HVO and standard diesel fuel were found negligible at room temperature but became slightly larger at high temperature. Moreover, most studies did not analyse the spray characteristics after the end of injection (EOI), which is also important to evaluate fuel spray at long ignition delay conditions, e.g., at the cold start conditions. Moreover, no quantitate correlation

between spray and experimental variables were previously obtained and reported by the researchers.

Several empirical models were thus developed by some other researchers [14, 24, 25]. Hiroyasu and Arai [25] divided the spray process into two periods by the breakup time. Results indicate fuel does not break up yet before the breakup time and thus fuel properties dominate the spray tip penetration during this period. After breakup time (usually at about 0.03ms ~ 0.1ms), the ambient conditions are dominant and the injection conditions (e.g. fuel injection pressure and fuel properties) become not comparable. Accordingly, they proposed a spray tip penetration model consisting of two equations to predict penetration before and after breakup time, as shown in Equation (9) and (10), which has been well-adopted in studies of many different biofuels. Nevertheless, the model was only validated at relatively low fuel pressure and low ambient pressure. Based on Hiroyasu and Arai 's principles, a detailed model named Naber and Siebers model [24] was formulated to include more parameters, but its results were proved insignificant to the spray penetration. In contrast, Bohl et al. [16] announced that fuel density should be considered and thus modified the Hiroyasu and Arai model to obtain better prediction on spray tip penetration under high fuel injection pressure conditions. However, all the models above did not analyse the significance of each parameter.

Design of experiments (DoE) is an experimental method including various approaches for designing experiments and analysing results based on mathematical statistics [26]. DoE method is popular in many research fields, which not only can effectively reduce the number of experiments but also correlate experimental variable to results with the analysis on the significance of each independent variable. Chen et al. [27] employed the Mixture Design Method (MDM) of DoE to formulate fuels and analyse the particulate matter emissions via a GDI engine. However, the MDM

is particularly for the design of compositions of mixtures but cannot be used in other fields involving independent variables. DoE was also introduced in the authors' previous work [28] where a semi-empirical model on the Sauter Mean Diameter (SMD) of spray by another approach named Response Surface Method (RSM). However, macroscopic characteristics of spray were not analysed in this work.

In summary, as a newly developed alternative fuel for diesel engines, the spray characteristics of HVO have not been thoroughly studied, especially those at post-injection period are rarely analysed. Meanwhile, most researches conducted on fuel spray did not cover all the impacts of fuel temperature, injection pressure, ambient temperature and ambient pressure, and did not independently control the ambient pressure and ambient temperature, which brings in difficulties in understanding the effect of ambient conditions. Moreover, previous models on spray penetration did not include enough variables such as fuel temperature and excluded the analysis on the significance of each variable. In addition, the DoE method showed advantages in designing conditions of experiments and formulating models with the analysis of variables. Accordingly, the influences of fuel conditions (fuel temperature and injection pressure) and ambient conditions (ambient pressure and ambient temperature) on the main macroscopic characteristics of HVO spray would be investigated via CFD simulation, which is validated by experimental data in a CVV. Furthermore, a new empirical model of spray tip penetration will be developed by fully analysing the significance of each factor by the RSM of DoE method.

2. Description of experiment processes

2.1. Test Rig

As shown in Fig. 1, the test rig contains a common rail fuel delivery system, optical diagnostic devices and a constant volume vessel (CVV). The common rail enables as high as 1800 bar fuel

pressure for injection. The CVV was designed to withstand internal air pressure and temperature at up to 100 bar and 1000 K respectively. A 4.5 kW heater is around the wall of the vessel and heats the internal air temperature to about 700K, which is measured by a type K thermocouple. A high-pressure nitrogen bottle provides up to 70 bar internal air pressure for the CVV. Four fused silica glass windows with 90 mm viewing size and 70 mm thickness are equally located on the wall for optical diagnostics. A LAUDA Integral XT 150 thermostat is connected to the CVV to prevent the temperature around windows exceeding 150 ℃. A single-hole solenoid injector with 0.16 mm orifice diameter is selected according to the specification of a Cummins ISB 4.5 diesel engine and installed at the top of the CVV. The injector is triggered by a TTL signal via a National Instrument data acquisition card PCI-6071E by a LabVIEW program. The main parameters of the CVV are shown in Table 1.

Table 1. List of key parameters of the CVV

Total internal volume	5.65 litres
Maximum working pressure	100 bar
Maximum working temperature	700 K
Heater	4.5KW, insulated, clamp on, ceramic band heater fitted with stainless steel cladding
Mounting style	Fixed vessel – removable cover
Materials	Inconel 625 gr 2 (vessel and cover) SA 479-316 Stainless steel (all other pressurised parts)

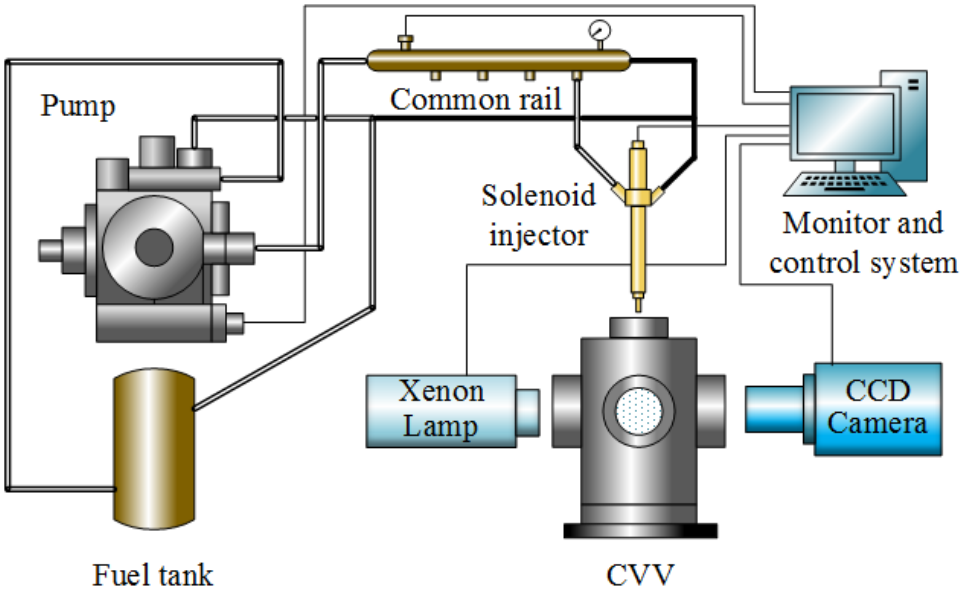

Fig. 1. The experimental system

The spray is observed through a window by a high-speed PHANTOM V710 CCD camera with a Nikon AF Zoom-Nikkor 24-85 mm f/2.8-4D lens, which is triggered by the same program for the injector. Due to the high frame rate of the camera, the exposure time is quite short (several microseconds) and the view of the camera is too dark to observe anything. Accordingly, a 100W lamp is installed on the other side to provide homogeneous background light via a diffuser film for observation during spray process. The internal pressure of the CVV is monitored by a Grems 3100b pressure transducer, and the internal temperature as well as the temperature of the windows and the heater are measured by K-type thermocouples. The accuracy of the pressure transducer and thermocouples are 1.5% and 0.75% respectively. A LabVIEW program receives these signals and automatically controls the heater and the temperature of the cooling water from the thermostat via serial interface RS232 protocol.

The hydrotreated vegetable oil (HVO) at 80 °C fuel temperature is injected at 1800 bar rail pressure, 100℃ ambient temperature and 70 bar ambient pressure. Its key properties are listed in Table 2.

Table 2. The main properties of HVO

Fuel type	Density (kg/m^3) at 15 °C	Viscosity (mm^2/s) 40 °C	Surface tension (N/m) at 40 °C	Aromatics content	Cetane number	LHV (kJ/kg)
HVO	780.1	3.02	0.0280	0	78	43902

2.2. Experimental procedures

In the experiment, the injection duration is 0.6ms, which is defined from the time when the injected fuel is visible to the time when the tail of the spray leaves the injector. The spray tip penetration is the length from the head to the tail of the liquid spray. The cone angle is defined according to literature [9], which is the angle formed by two lines from the tail of the spray to the outer periphery of the spray at 1/3 length of the spray tip penetration, as shown in Fig. 4. The start time of the injection is defined as the start of injection (SOI), and the end can be named the end of injection (EOI). The time before and after the EOI can be respectively called the injection and post-injection periods. **Fig. 2** shows the injection rate of the injector at 1800 bar rail pressure. The camera is set to 256 × 256 pixels resolution at a sample rate of 50,000 fps and exposure time of 19 μs to capture the image of spray with the interval of 0.02ms. The sample time is 1ms for the experiment. When the internal pressure and temperature stay at 70 bar and 100℃ respectively, a LabVIEW program is running to trigger the injector and the camera simultaneously. Then, the fuel is injected into the CVV and the camera starts to capture images every 0.02 ms. Therefore, 30 images of spray can be obtained for the injection (0 ~ 0.6 ms), and 20 images are obtained for the post-injection (0.6 ~ 1 ms). These images are displayed on a computer and the spray tip penetration and cone angle are measured by the image processing software.

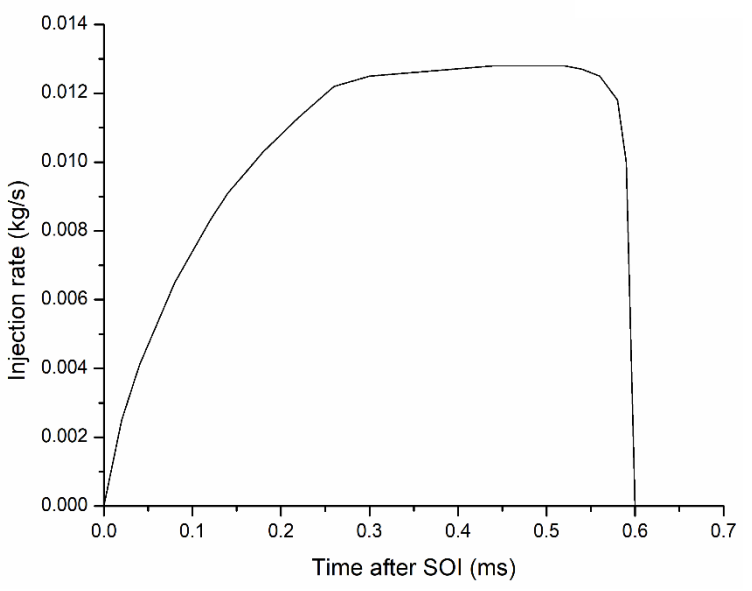

Fig. 2. Injection rate at the rail pressure of 1800 bar

3. Numerical methodologies

3.1. Breakup models

Two breakup models have been developed for liquid fuel spray and combustion in diesel engines. The Wave breakup model of Reitz is appropriate for high-speed fuel injections, which considers the droplets breakup is induced by the relative velocity between the gas phases and the liquid phases. During the breakup, the Kelvin-Helmholtz instability is assumed to be dominant, and the size of child droplets is proportional to the wavelength of the unstable surface wave on the parent droplet, as shown in Equation (1) [29].

$$r = B_0 \Lambda \tag{1}$$

Where r is the radius of the child droplet, B_0 is constant and usually set to 0.61 according to Reitz's work [30]. The changing rate of the radius of the droplet is given by

$$\frac{da}{dt} = -\frac{(a-r)}{\tau}, \; r \leqslant a \tag{2}$$

Where a is the radius before breakup and τ is the breakup time determined by

$$\tau = \frac{3.726 B_1 a}{\Lambda \Omega} \quad (3)$$

B_1 is the breakup time constant and it determines how quickly the parcel will lose mass [29]. Ω is the maximum growth rate and Λ is the corresponding wavelength of parent droplet, which can be calculated by

$$\frac{\Lambda}{a} = 9.02 \frac{(1+0.45Oh^{0.5})(1+0.4Ta^{0.7})}{(1+0.87We_2^{1.67})^{0.6}} \quad (4)$$

$$\Omega \sqrt{\frac{\rho a^3}{\sigma}} = \frac{0.34+0.38We_2^{1.5}}{(1+Oh)(1+1.4Ta^{0.6})} \quad (5)$$

Where $Oh = \sqrt{We}/Re$ is the Ohnesorge number, $Ta = Oh\sqrt{We}$ is the Taylor number and $Re = \rho U^2 \mathrm{a}/\sigma$ is the Reynolds number. The footnote 1 and 2 mean the liquid phase and the gas phase respectively.

The KHRT breakup model is usually for high Weber number sprays, and thus also commonly used for diesel spray and combustion. It considers both the impact of Kelvin-Helmholtz waves driven by aerodynamic forces and the effect of Rayleigh Taylor instabilities caused by the acceleration of shed drops. Both mechanisms describe droplet breakup by tracking wave growth on the surface of the droplet and believe breakup occurs due to the local fastest growing instability. The KHRT breakup model also assumes that a liquid core exists in the near-nozzle region and introduces the Levich core length to model the breakup due to Kelvin-Helmholtz wave growth [18].

In the KHRT breakup model, child droplets are shed from the liquid core in the near-nozzle region and experience sudden acceleration when ejected into the freestream. The length of the liquid core (Levich core length) is obtained by:

$$L = C_L d_L \sqrt{\frac{\rho_l}{\rho_g}} \quad (6)$$

Where C_L is the Levich constant which is a reference nozzle diameter. The Rayleigh-Taylor (RT) model is based on wave instabilities on the droplet surface. And the number of the fastest growing wave is

$$K_{RT} = \sqrt{\frac{-g_t(\rho_p - \rho_g)}{3\sigma}} \quad (7)$$

g_t here is the droplet acceleration along the droplet track.

The radius of the child droplets can be obtained by:

$$r_c = \frac{\pi C_{RT}}{K_{RT}} \quad (8)$$

where C_{RT} is the breakup radius constant.

3.2. Model setup

A 2D geometric model is built and imported to ANSYS Fluent 18.1 to simulate spray in the CVV. 180628 structural cells are drawn in the fluid domain. The surface injection is selected for the injection type, and the orifice diameter of the fuel inlet is 0.16 mm. The mass flow rate of fuel is set according to **Fig. 2**. The condition in the model is set to the same as that in the experiment. Both the Wave model and the KHRT model are selected as the breakup models. The breakup constants B_0 and B_1 are 0.61 and 20 in the Wave model, as literature [17] demonstrated that these values enable the model to predict the spray tip penetration and the SMD well simultaneous for spray and combustion in the diesel engine. To the KHRT model, literature [31] recommended to set the B_0 and B_1 to 0.61 and 18 because the configuration was proved to predict the spray tip penetration, local droplet size and droplet velocity with high accuracy. The initial droplet diameter at the inlet is set to 0.16mm, and the dynamic-drag is employed as the drag law. The RNG k-ε model and the Standard Wall Functions are selected for the viscous model and the near-wall treatment. The main properties of HVO at various temperature come from literature [23].

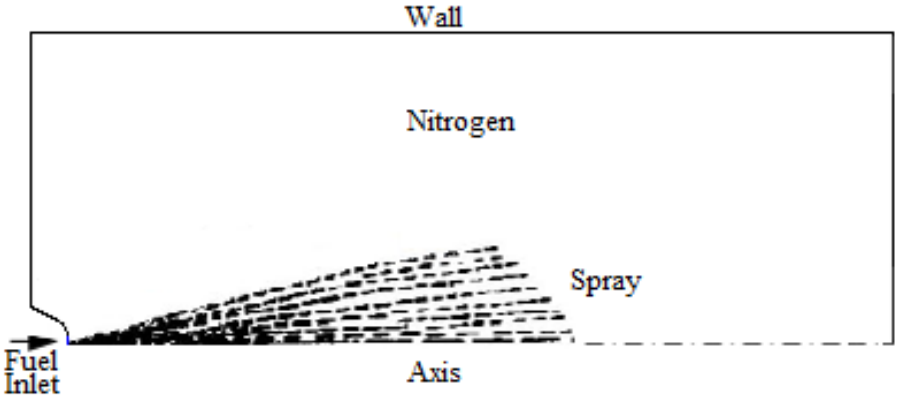

Fig. 3. Diagram of the CVV model

4. Design of operating conditions

As aforementioned, Hiroyasu et al. [25] proposed the model of the spray tip penetration in the following equations:

$$S_1 = 0.39 \cdot \left(\frac{2 \cdot \Delta P}{\rho_f}\right)^{\frac{1}{2}} \cdot t \qquad \text{when } t < t_b \qquad (9)$$

$$S_2 = 2.95 \cdot \left(\frac{\Delta P}{\rho_a}\right)^{\frac{1}{4}} \cdot \sqrt{d_0 \cdot t} \qquad \text{when } t \geq t_b \qquad (10)$$

Where ΔP is the pressure drop across the outlet of the injector, ρ_f is the density of the fuel, ρ_a is the density of the air, and d_0 is the inner diameter of the injector. t refers to the time after the SOI and t_b is the breakup time. S_1 and S_2 are the length of spray tip penetration before and after the breakup, respectively.

Since the model of S_1 is of high accuracy, only the model of S_2 is being discussed here. As known, ρ_a can be obtained by the ambient temperature T_a and ambient pressure P_a, and the pressure drop ΔP is determined by the common rail pressure P_r and ambient pressure P_a. Therefore, the spray tip penetration can be formulated by the rail pressure P_r, the ambient pressure P_a, the ambient temperature T_a, the inner diameter of the injector d_0 and time after SOI t. In this research, d_0 is constant, and thus Equation (10) can be re-written as:

$$S_2 = a \cdot {P_r}^b \cdot {P_a}^c \cdot {T_a}^d \cdot t^e \quad (11)$$

Where a, b, c, d and e are constant and will be obtained by calculations. According to the specifications of the CVV, the ranges of main parameters are listed in **Table 3**.

Table 3. The range of typical parameters

P_r (bar)	T_f (K)	P_a (bar)	T_a (K)	t (ms)	d_0 (mm)
600, 1800	300 ~ 500	10 ~ 70	300 ~ 700	0.1 ~ 1	0.16

In order to reduce the times of calculations, Design of Experiments (DoE) is adopted in this work to design the operating conditions. Equation (11) can be logarithmically transferred to:

$$\log S_2 = a + b \cdot \log P_r + c \cdot \log P_a + d \cdot \log T_a + e \cdot \log t \quad (12)$$

The operating conditions for the CFD simulation can be obtained by the Response Surface Method (RSM) in DoE and are shown in logarithmic value.

Table 4. Operating conditions

Conditions	$\boldsymbol{P_r}$ (bar)	$\boldsymbol{T_f}$ (K)	$\boldsymbol{P_a}$ (bar)	$\boldsymbol{T_a}$ (K)
1	600	300	70	700
2	600	300	10	300
3	600	300	70	300
4	600	300	10	700
5	600	300	26	458
6	600	387	10	458
7	600	387	26	458
8	600	387	26	300
9	600	387	26	700
10	600	387	70	458
11	600	500	26	458
12	600	500	70	300
13	600	500	10	700
14	600	500	10	300
15	600	500	70	700
16	1800	300	10	700
17	1800	300	70	300

18	1800	300	70	700
19	1800	300	26	458
20	1800	300	10	300
21	1800	387	26	458
22	1800	387	26	700
23	1800	387	70	458
24	1800	387	10	458
25	1800	387	26	300
26	1800	500	10	700
27	1800	500	10	300
28	1800	500	70	300
29	1800	500	70	700
30	1800	500	26	458

5. Results and discussion

5.1. Model validation

The CFD model was run under the same condition as the experiments. **Fig. 4** illustrates the spray obtained by experimental and numerical method (Wave model) at 0.6ms after SOI, which also indicates the definition of the spray tip penetration and cone angle. Fig. 5 and Fig. 6 show the comparison of cone angle and spray tip penetration after SOI between experiments and the two breakup models at 1800 bar rail pressure, 100℃ ambient temperature and 70 bar ambient pressure.

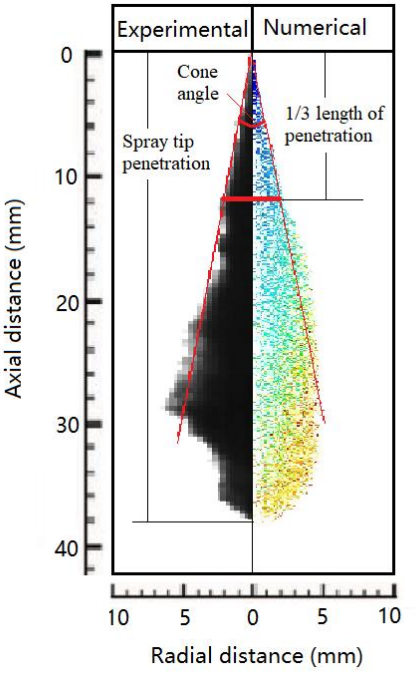

Fig. 4. The comparison between the experimental and numerical (Wave model) spray at 1800 bar rail pressure, 100℃ ambient temperature and 70 bar ambient pressure

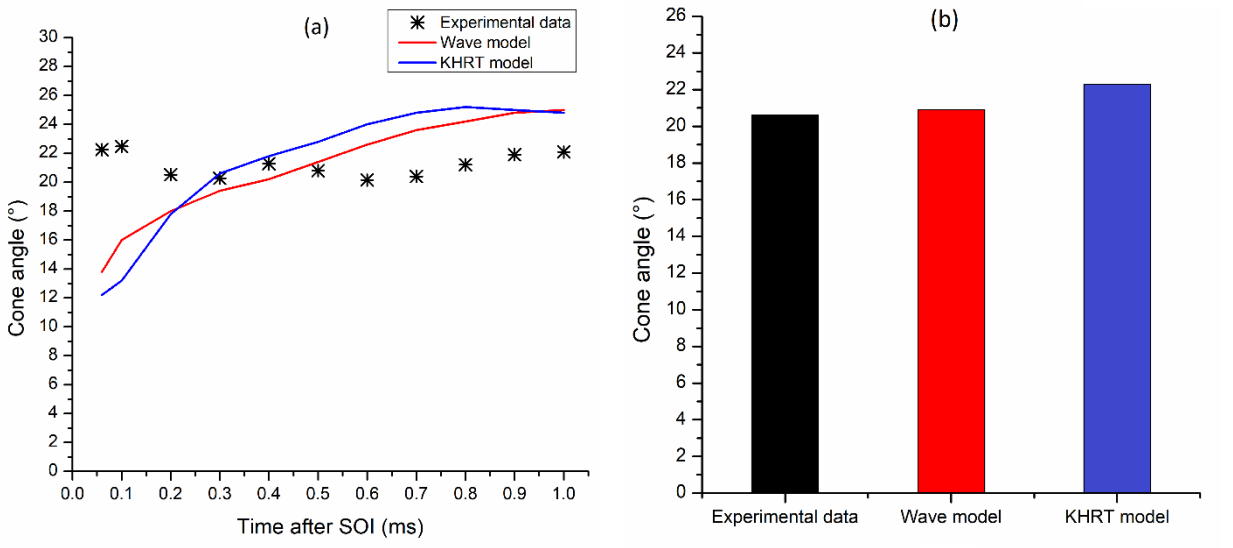

Fig. 5. Comparison of cone angle (a) and average cone angle (b) between experimental and numerical results

As shown in **Fig. 5** (a), the experimental cone angle fluctuates and reaches its peak at about 0.1ms but stays within the range of 20.1° to 22° after 0.3ms. It indicates that the spray is not stable until about 0.3ms, as the flow rate of the injector is still increasing dramatically in this period. Literature [13] also explains that the time of the peak cone angle is the breakup time, before which the spray is yet fully developed and has a blob-like shape resulting in larger cone angle. In contrast, the predicted cone angles by the two breakup models both increase with sample time. It is probably attributed to the different impact of rail pressure on actual spray and the two breakup models. On one hand, previous research [10] demonstrates that the cone angle is not sensitive to injection pressure. On the other hand, both the Wave model and the KHRT model consider the effects of Kelvin-Helmholtz waves, which are probably to be influenced by the injection pressure.

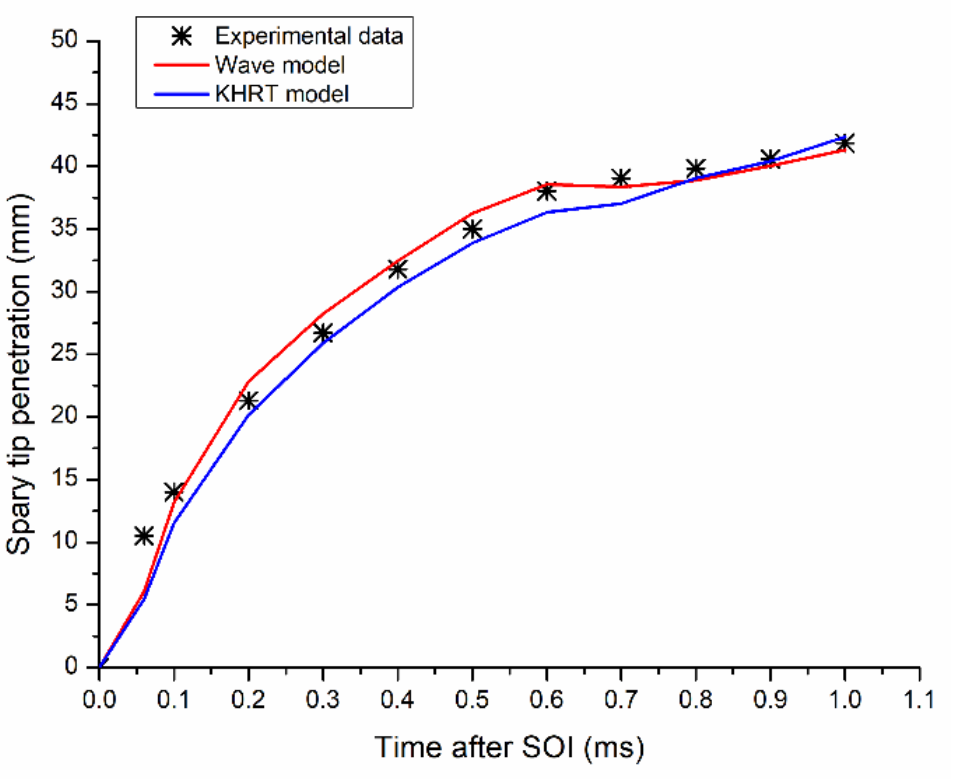

Fig. 6. Comparison of spray tip penetration between experimental and numerical methods

As shown in **Fig. 6**, the spray tip penetration obtained by experiments increases with sample time but the increasing rate is reducing. Spray tip penetrations predicted by both the Wave breakup model and the KHRT breakup model agree with the experimental data well. The bias of Wave model is within 10% in the whole duration except that before 0.1 ms, the breakup time, whilst the bias of KHRT model is slightly larger. Both models under-estimate penetration before breakup because the two models are both for secondary breakup whilst the actual breakup in this period still has not begun, which means less energy loss happens to droplets in actual spray than the predicted spray. During 0.6ms ~ 0.7ms, the penetration predicted by the Wave model experienced slight drop whilst that predicted by the KHRT model and the experimental data both grow slightly. It is possibly because the Wave model is mainly used for high-speed injections but the actual speed

in this period reduced dramatically. Consequently, the actual droplet breakup significantly decays and results in shorter penetration than the predicted one by the Wave model. And the bias should only occur at relatively high ambient pressure and low ambient temperature, where the breakup is fiercer and changes more sharply once the injection stops.

Consequently, as recommended in previous study [13], the average cone angle between 0.3 ms and 0.6 ms is employed as a factor indicating spray quality in this study because the cone angle is relatively stable in this duration and the error of the predicted average cone angle for this period is also acceptable as shown in Fig. 5 (b). Meanwhile, the predicted data of spray tip penetration from breakup time (no earlier than 0.1ms) is analysed by the Wave breakup model in the paper due to its higher precision.

5.2. Macroscopic characteristics of spray

Only the Wave breakup model is used to predict the spray tip penetration and cone angle. As known, the spray tip penetration and cone angle are the most important macroscopic characteristics indicating the quality of spray, which is mainly determined by the breakup and evaporation of droplets. The breakup is a process breaking the balance between the dynamic force of the droplet and the viscosity and surface tension of the droplet. The dynamic force is determined by the momentum of droplets and the interaction with ambient gas. Therefore, penetration can be likely promoted by higher droplets velocity and higher fuel properties such as density, viscosity and surface tension, and reduced by higher ambient gas density and higher evaporation rate. In contrast, larger cone angle always occurs when a stronger breakup happens, but the evaporation may result in smaller cone angle. Usually, the shorter penetration and larger cone angle are expected for spray combustion in a diesel engine.

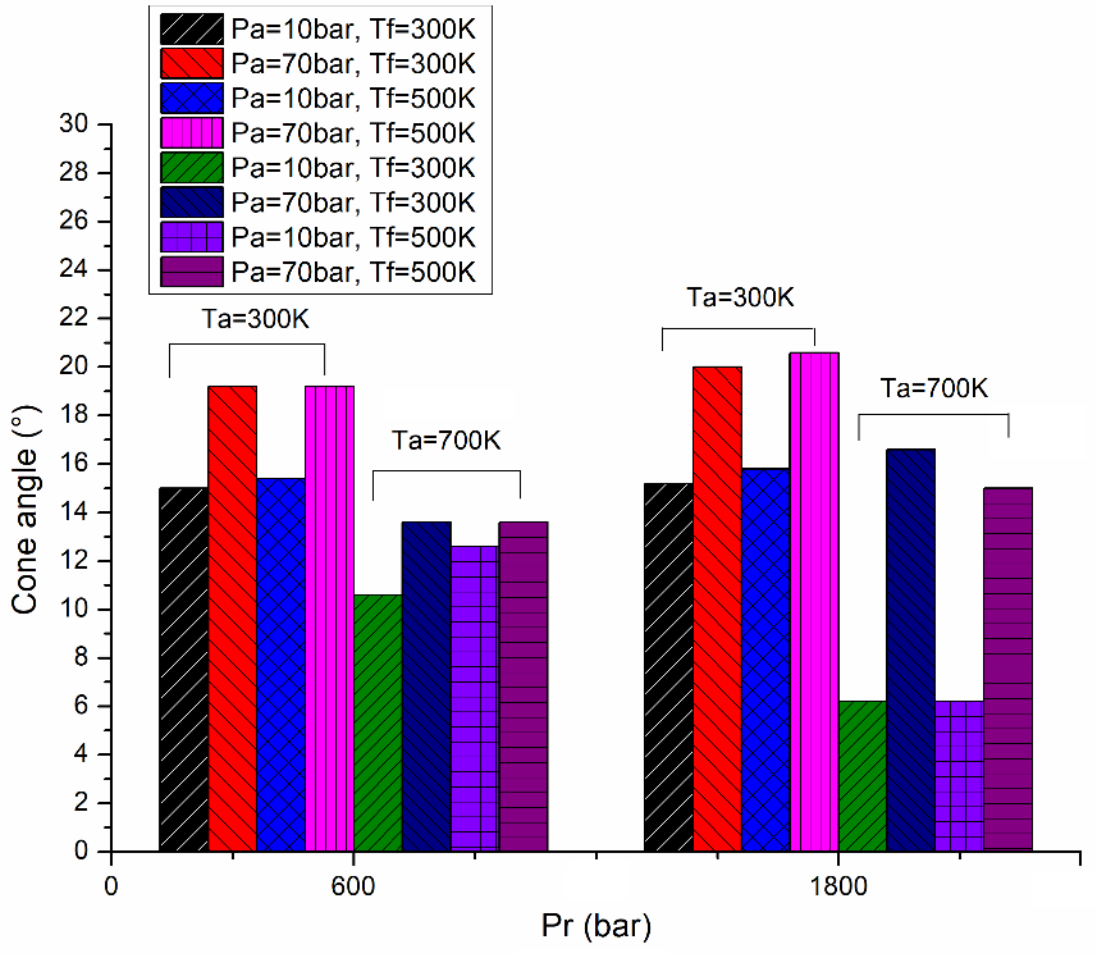

Fig. 7. Average cone angle at various conditions

As cone angle is a relatively stable value against sample time during the injection, only the average cone angle between 0.3ms and 0.6ms after the SOI is considered to stand for the quality of spray, as shown in **Fig. 7**. At cold ambient condition (T_a=300K), the cone angles at 1800 bar rail pressure are only slightly higher than those at 600 bar rail pressure and those at high ambient pressure are always smaller than those at low ambient pressure, which means ambient pressure is dominant and the impact of rail pressure on cone angle is not significant at cold ambient condition. However, the cone angle at hot ambient condition (T_a=700K) shows two different phenomena: the cone angle at 1800 bar rail pressure is much smaller than that at 600 bar when the ambient pressure is 10 bar,

whilst the tendency is opposite when the ambient pressure is 70 bar. It indicates that at the hot ambient condition, the effect of evaporation is more important at low ambient pressure, which is exceeded by that of breakup when ambient pressure rises. The fuel temperature has no impact on the cone angle under most conditions, except that at 70 bar ambient pressure and 700K ambient temperature, where a smaller cone angle occurs due to faster evaporation of hot fuel (500K).

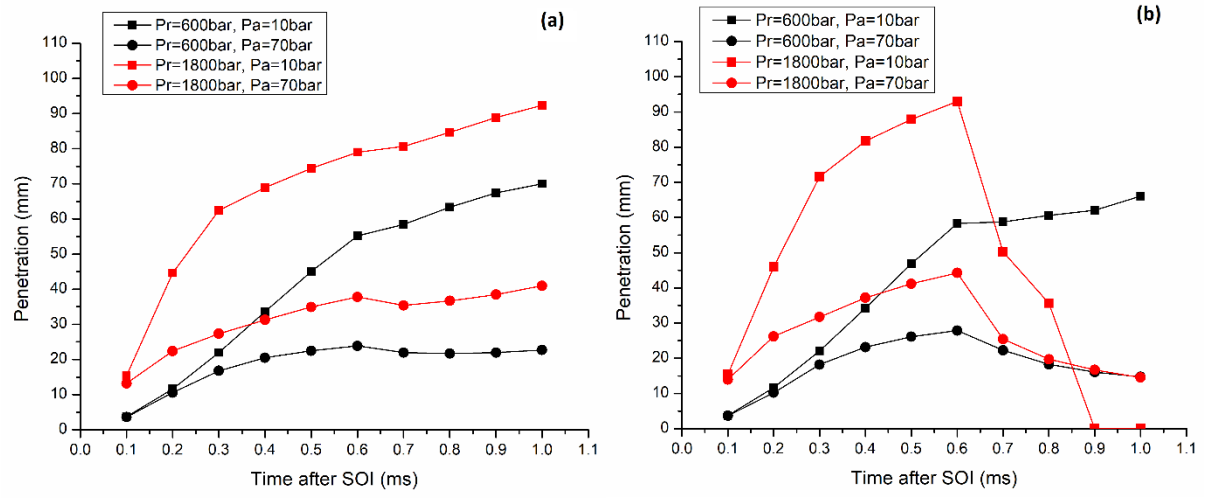

Fig. 8. Effect of ambient pressure on spray tip penetration

(a) T_f =300K, T_a=300K (b) T_f=300K, T_a=700K

Fig. 8 (a) and (b) indicates the spray tip penetration increase with sample time during the injection (0.1ms ~ 0.6ms) under all conditions, and the ambient pressure has an obviously negative impact on spray tip penetration. During the injection, the penetration at 10 bar ambient pressure is always much higher than that at 70 bar, due to its higher velocity of droplets. Moreover, the increasing rates of penetration at 1800 bar rail pressure are all higher than those at 600 bar at the beginning of injection (before 0.3ms) when the ambient pressures are 10 bar, whilst both rail pressures are almost the same during injection when the ambient pressure is 70 bar. The phenomena reveal that higher ambient pressure is beneficial to atomization. According to the force analysis of droplet,

the higher density of the ambient gas (nitrogen) at high ambient pressure brings much larger dynamic drag force to droplets and thus promote droplets breakup to smaller droplets, whilst the impact of ambient pressure on droplet viscosity and surface tension is neglectable. It also agrees with the results in previous work [32], where the impinging effect was found dominant in breakup process. When the ambient pressure is 10 bar, the more injected fuel mass and higher initial velocity of droplets have the more significant impact on penetration than the ambient gas. However, when droplets eject to downstream, the impact of rail pressure decays and that of ambient pressure becomes dominant, which reduces the increasing rate of penetration after the EOI at the cold ambient condition, as shown in **Fig. 8** (a). In contrast, the impact of ambient gas at 70 bar is much stronger determines the droplet breakup at the cold condition. Therefore, the increase rate of penetration at two different rail pressures is similar to each other in **Fig. 8** (a). In general, when the ambient temperature is not high, the rail pressure dominates the fuel spray at the beginning of injection at low ambient pressure because it determines the initial velocity of droplets, whilst the high ambient pressure is more significant at both rail pressures during the whole injection due to its impact on droplets breakup.

In the post-injection period (after 0.6ms), the tendencies of penetration are more complicated because the impact of temperatures (fuel and ambient gas) also arises. At low temperatures, penetrations at low ambient pressure (10 bar) keep increasing with similar rates regardless of rail pressure. However, at high ambient pressure (70 bar) penetrations only increase slightly, as shown in **Fig. 8** (a). It indicates that the evaporation effect is not significant, so the fuel droplets can still penetrate forward driven by inertia and impacted by the ambient pressure. The penetrations at high ambient pressure both experience slight drop during 0.6ms ~0.7ms, similar to that in Fig. 6, which is caused by the bias on the breakup of Wave model. With the temperature increasing, the

penetrations at the two rail pressure show different tendencies. As shown in **Fig. 8** (b), penetrations at 1800 bar rail pressure view dramatic drop at all ambient pressures after the EOI, whilst those at 600 bar rail pressure convert from a slight increase to gradually decrease. These phenomena reveal that evaporation plays the most important role in the post-injection period because the droplets have a rather low velocity and thus the impact of the rail pressure and ambient pressure weakens. As droplets at higher rail pressure and ambient pressure have smaller size due to more drastic breakup before EOI and thus become vapour sooner after the EOI than those at lower rail pressure and ambient pressure. Different increasing and decreasing rates at ambient pressure are mainly caused by the different droplet velocities at the EOI.

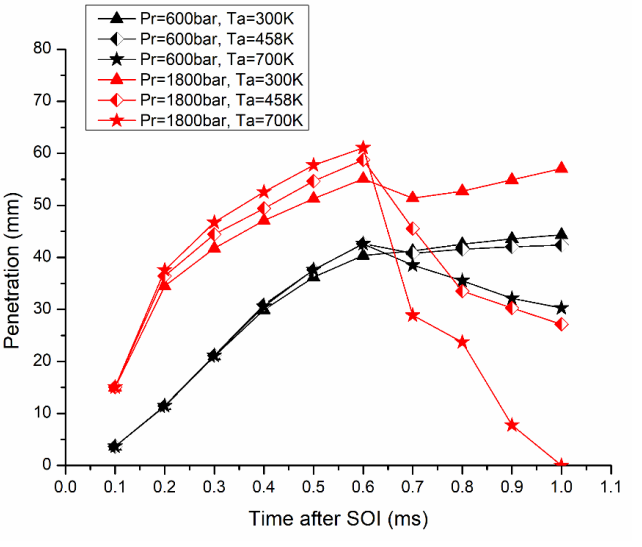

Fig. 9. Effect of ambient temperature on spray tip penetration when T_f=387K and P_a=26 bar

The effect of ambient temperature on spray tip penetration at 387 K fuel temperature and 26 bar ambient pressure is shown in **Fig. 9**. Results indicated the penetrations all increased with sample time during injection but shown different tendencies after the EOI. During injection, penetrations at 1800 bar rail pressure increase with increasing ambient temperature during the injection, whilst

those at 600 bar rail pressure have no obvious difference in this period. It indicates that the fuel injected at 1800 bar can penetrate longer distance at higher ambient temperature because the density of ambient gas decreases at the higher temperature and constant pressure. Nevertheless, the effect of ambient temperature is not significant when the rail pressure is low because the initial droplet velocity is not high enough so that the impact of ambient gas density on droplets is not significant. It is also shown in **Fig. 9** that penetrations at both rail pressures change from a slight increase to sharp drop with increasing ambient temperature after the EOI and the decreasing rate is larger at higher rail pressure. It means ambient temperature becomes the dominant factor in the post-injection period, which is probably because droplets can no longer break up after the EOI and only evaporate and diffuse to the ambient gas. The larger decreasing rate of penetration at 1800 rail pressure is due to the smaller droplet size produced by more severe breakup during injection.

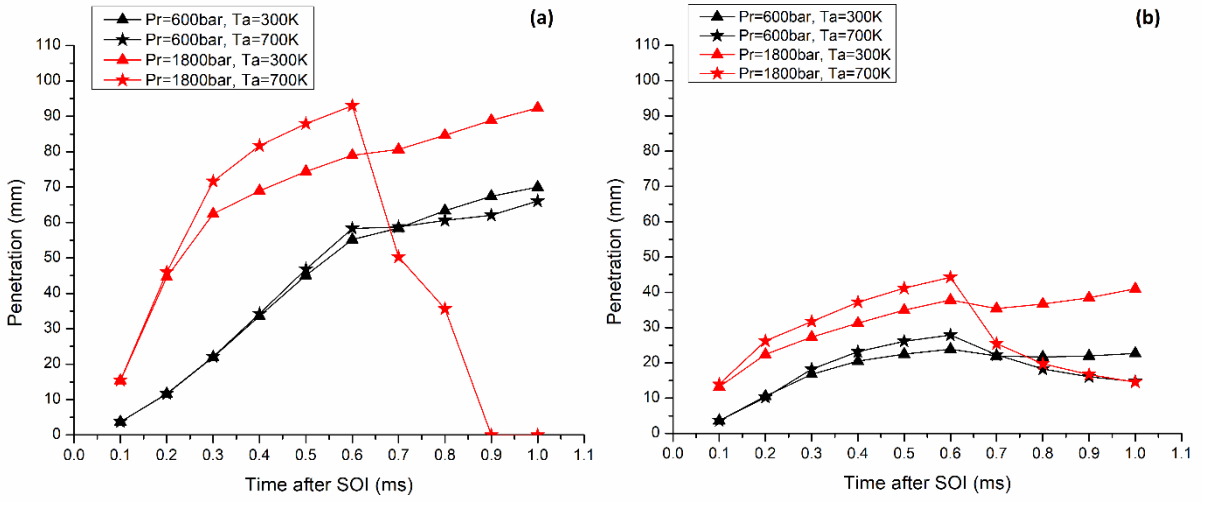

Fig. 10. Effect of ambient temperature Spray tip penetration

(a) T_f=300K, P_a=10 bar (b) T_f=300K, P_a =70 bar

When the ambient pressure reduces to 10 bar (a) or increases to 70 bar (b), the impact of ambient temperature on penetrations of fuel injected at 1800 bar is quite similar as shown in the Fig. 10:

penetration at higher ambient temperature is longer than that at lower ambient temperature during the injection, and then the penetration at lower ambient temperature keeps increasing gradually but that at high temperature decreases dramatically. As the density of ambient gas reduces with increasing temperature at constant pressure, the dynamic drag force on injected fuel droplets is becoming weaker and thus results in longer penetration. Meanwhile, as the velocity of the droplet during injection is quite high, the amount of evaporated fuel is not comparable in such short duration. After the injection, the velocity of droplets slows down soon at high ambient pressure and then evaporation starts to play a more important role in penetration proceeding, whilst the impact of evaporation is comparable with that of ambient pressure at 10 bar because the velocity of droplets is higher and decreases slower under this condition.

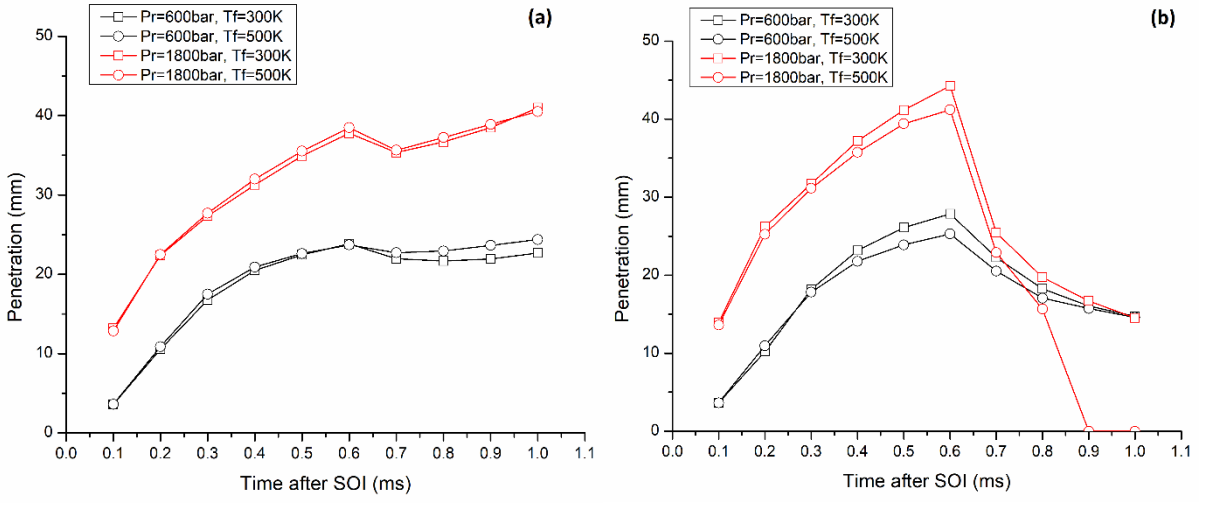

Fig. 11. Effect of fuel temperature on spray tip penetration

(a) P_a=70 bar, T_a=300K (b) P_a=70 bar, T_a=700K

From **Fig. 11** (a), the penetrations at the two different fuel temperatures are almost the same at either rail pressure during injection, because the velocity of the droplet is fast, and the ambient temperature is low (300K). As a result, the dynamic force on droplets is dominant compared to the

small evaporation rate under this condition. After the EOI, the penetrations at 1800 bar rail pressure do not show the difference with varying fuel temperature, because the initial droplets velocity during post-injection is still very high at 1800 bar rail pressure. However, fuel injected at 600 bar has different penetrations, which increase slightly at high fuel temperature instead of decreasing. It is inferred that the hot droplets warm up the local ambient gas and thus the density of ambient gas around the droplets reduces slightly and results in a bit longer penetration.

In contrast, when the ambient temperature is 700 K in **Fig. 11** (b), the effect of evaporation is significantly enhanced and becomes dominant after the EOI. Consequently, the penetrations in the injection period experience a slight decrease with increasing fuel temperature and the decrease becomes more significant in the post-injection period reduce at both rail pressures.

6. DoE models of spray tip penetration

As previously discussed, the penetration model after the breakup time is formulated by DoE method to correlate independent variables (rail pressure, fuel temperature, ambient pressure and ambient temperature) to response (spray tip penetration). Given the results above, spray tip penetrations before and after the end of injection (EOI), which can also be called injection and post-injection respectively, are quite different. Therefore, two models were formulated for penetrations in the two periods (except those before breakup). As shown in Table 5, an analysis of variance (ANOVA) is thus performed to investigate the fitness and significance of the formulated models and each variable.

Table 5. ANOVA of experimental factors and the models

Factor	R1		R2	
	F-value	P-value	F-value	P-value
Model	525.17	0.0001	82.31	0.0001
A	522.59	0.0001	not significant	not significant

B	not significant	not significant	3.24	not 0.0738
C	158.89	0.0001	220.86	0.0001
D	3.43	0.0657	65.20	0.0001
E	1416.64	0.0001	39.71	0.0.0001
R^2	0.9231		0.6942	
Adj R^2	0.9213		0.6858	
Pred R^2	0.9180		0.6686	
Adeq Precision	86.142		35.071	

The factor A, B, C, D and E are the rail pressure (P_r), fuel temperature (T_f), ambient pressure (P_a), ambient temperature (T_a) and the sample time (t), whilst the R1 and R2 stand for the spray tip penetration before and after the EOI. The F-value represents the comparison between the model variance (Regression) and its residual (error) variance. A high F-value (>1) is acceptable because it means the regression is much larger than the residual. The P-value is the probability that a factor has no effect on the response even though the F-value is high. A P-value of less than 0.05 means the factor is significant to the response, but a P-value larger than 0.1 implies the factor is insignificant. Usually, it is overall significant when the P-value of a model is less than 0.05 and that of each factor is less than 0.1. In this study, the models have the F-value of 525.17 and the P-value of 0.0001 to R1, whilst those of R2 are 82.31 and 0.0001 respectively. It means the model is significant to predict the spray tip penetration during injection and post-injection periods, and only 0.01% chance that the F-values of 525.17 and 82.31 occur due to noise. Moreover, factors A, C and E all have large F-values and small P-values to R1, which indicates the spray tip penetration during injection is significantly impacted by the rail pressure (P_r), ambient pressure (P_a) and sample time (t). Similarly, the rail pressure (P_r), ambient pressure (P_a), ambient temperature (T_a) and sample time (t) have a significant impact on the spray tip penetration in the post-injection period because the F-values are all larger than 1 and P-values are all smaller than 0.1.

The R^2 is a measure of the amount of variation around the mean explained by the model, and the Adj R^2 is that adjusted to compensate for the addition of variables to the model. High R^2 (close to unity) and Adj R^2 are acceptable for the model. The Pred R^2 is used to measure how good the model can predict new response values. The model is statistically sound if the difference between the Pred R^2 and Adj R^2 is within 0.2. The Adeq Precision is a signal-noise ratio and is usually desirable when it is larger than 4 [33]. In this research, the models of R1 and R2 have high R^2, Adj R^2 and Adeq Precision, and the differences between the Pred R^2 and Adj R^2 are small, which indicates the two models are accurate in predicting the spray tip penetrations at both injection and post-injection periods.

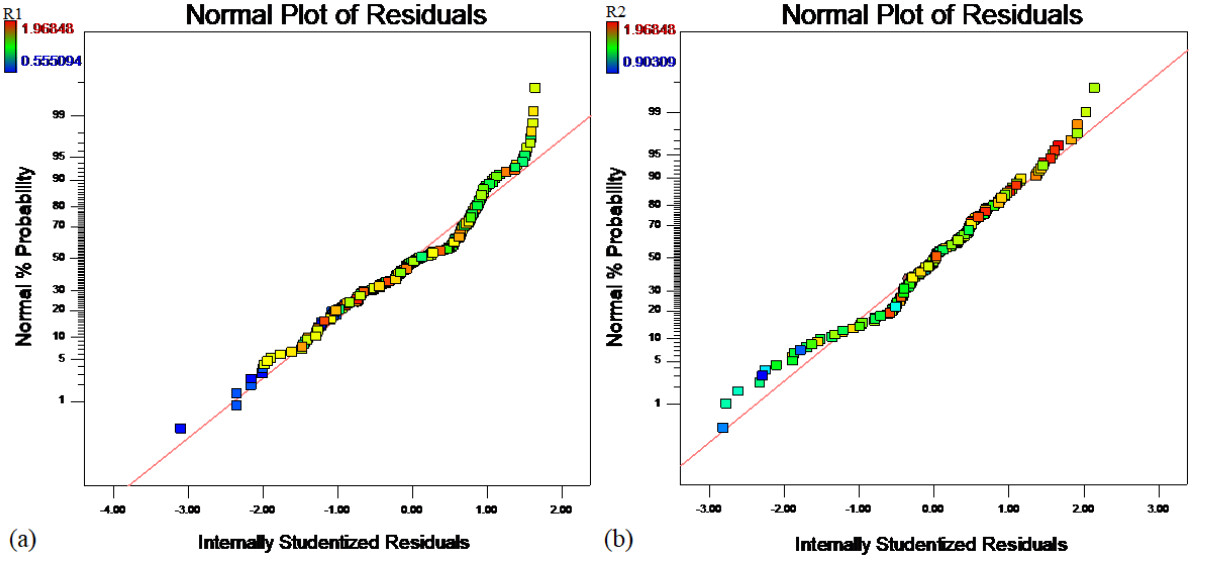

Fig. 12. Normal probability plots of residuals for R1 (a) and R2 (b)

The normal probability plot in **Fig. 12** indicates whether the residuals follow a normal distribution, where the points follow a straight line. **Fig. 12** shows that the points of R1 and R2 narrowly scatter around the straight lines. It reveals that the residuals for R1 and R2 follow normal distributions

well and the derived models will not be improved by any transformation to R1 and R2, which in other words means the models are valid.

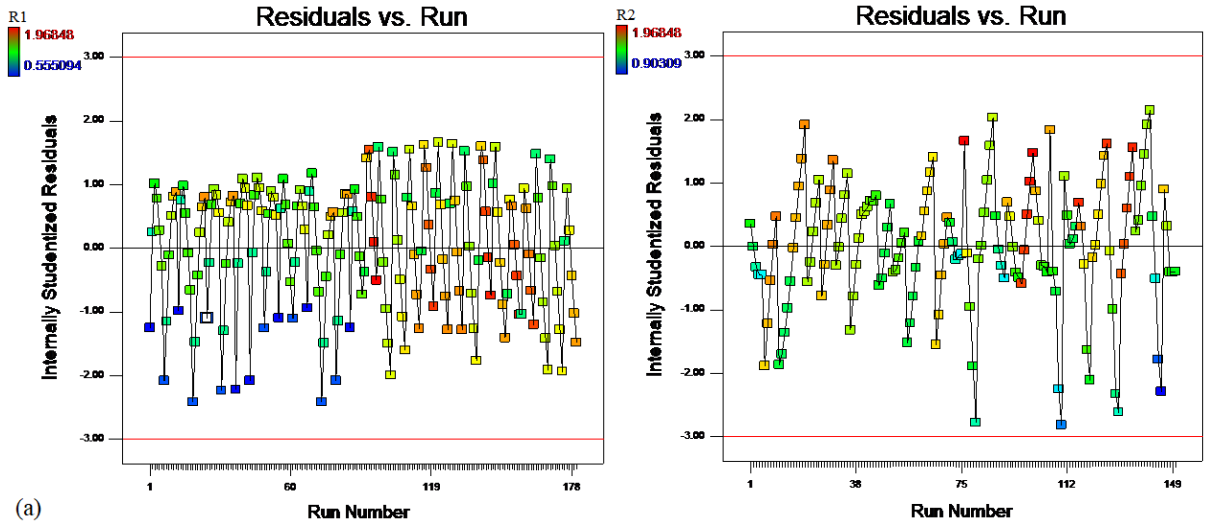

Fig. 13. Residuals of R1 (a) and R2 (b) versus the run order

The residuals versus run plots are employed to find lurking time-related variables that may influence the response. A random scatter means no systematic effect on the response is caused by the run order and is thus desirable. As shown in **Fig. 13**, the residuals of R1 and R2 have no evident trends associated with the run order, which reveals the possibility can be excluded that R1 and R2 are impacted by any time-dependent factors.

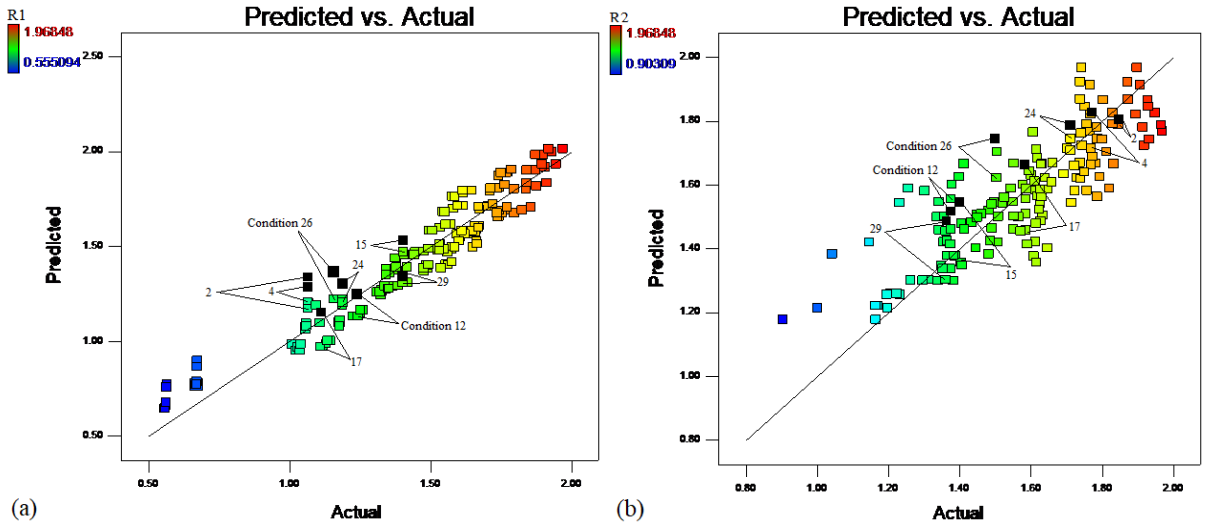

Fig. 14. The predicted values of R1 (a) and R2 (b) versus actual values

Fig. 14 is the comparison between the actual values and predicted values by the DoE models of R1 and R2. It means the models are precise if most scatter points are located closed to the central line in the graphs. According to the distribution of the coloured point in Fig. 14, the derived DoE models are precise to predict R1 and the precision for R2 is lower.

After the analysis of variance (ANOVA) and the diagnostics, the coded Equation (13) and (14) are obtained to quantitively analyse the effect of each factor on responses regardless of its unit. In the coded equations, factors A, B, C, D and E are coded to the interval of [-1, 1] as shown in Table 6.

Table 6. The coded factors and the levels in the analysis on R1 and R2

Variable	Factor	R1		R2	
		-1	1	-1	1
$\log_{10} P_r$	A	2.778	3.255	2.778	3.255
$\log_{10} T_f$	B	2.477	2.699	2.477	2.699
$\log_{10} P_a$	C	1	1.845	1	1.845
$\log_{10} T_a$	D	2.477	2.845	2.477	2.845
$\log_{10} t$	E	-1	-0.223	-0.223	0

$$R_1 = 1.33 + 0.16 \cdot A - 0.11 \cdot C + 0.016 \cdot D + 0.4 \cdot E \quad (13)$$

$$R_2 = 1.57 - 0.022 \cdot B - 0.18 \cdot C - 0.1 \cdot D - 0.09 \cdot E \quad (14)$$

The coefficients of the coded equations stand for the importance of corresponding factors: A positive value indicates a synergistic effect, whilst a negative value means an antagonistic effect, and the absolute value indicates the significance to the R1 and R2. As illustrated in the coded equations, factor A has a synergistic effect on R1 but no impact on R2, whilst C has an antagonistic effect on them both. D is the most significant factor in reducing R2 but slightly increasing R1. These phenomena also agree with the results in Fig. 8 ~ Fig.11.

The uncoded models reveal the actual correlation between the spray tip penetration and independent variables

$$\log_{10} \mathrm{S} = 0.034177 + 0.6813 \cdot \log_{10} P_r - 0.25976 \cdot \log_{10} P_a + +0.087668 \cdot D + 1.01863 \cdot \log_{10} t, \quad t_b < t < t_{EOI} \quad (15)$$

$$\log_{10} S = 4.05892 - 0.20026 \cdot \log_{10} T_f - 0.43379 \cdot \log_{10} P_a - 0.54129 \cdot \log_{10} T_a - 0.80936 \cdot \log_{10} t, \quad t > t_{EOI} \quad (16)$$

Where P_r, T_f, P_a, T_a and t refer to the rail pressure (bar), fuel temperature (K), ambient pressure (bar), ambient temperature and sample time. S refers to the spray tip penetration. The t_b and t_{EOI} are the time of breakup and the end of injection (EOI) respectively. Therefore, the final form of the spray tip penetration models can be described below:

$$S = 1.0819 P_r^{0.6813} P_a^{-0.25976} T_a^{0.087668} t^{1.01863}, \quad t_b < \mathrm{t} < t_{EOI} \quad (17)$$

$$S = 11453.0195 T_f^{-0.20026} P_a^{-0.43379} T_a^{-0.54129} t^{-0.80936}, \quad \mathrm{t} > t_{EOI} \quad (18)$$

The main differences between the DoE models and other empirical models are twofold: first, the DoE models can describe the spray tip penetration during the post-injection period; second, the effect of evaporation is taken into account in the DoE model as it include the factor of ambient temperature and fuel temperature. Fig. 14 also compares the precision of the DoE model and the Hiroyasu model, where the black scatter points are the results of the Hiroyasu model and the coloured ones are the DoE model. As Fig. 14 is the comparison between the predicted values by models and the actual values, more closed location of the points to the central line usually indicates a more precise model. Accordingly, at cold ambient condition (e.g., Condition 12, 17 and 29), where the evaporation is not significant, the DoE model has lower precision than the Hiroyasu model. However, when the ambient temperature rises and evaporation becomes significant (e.g., Condition 2, 4, 15, 24 and 26), the precision of DoE model exceed that of Hiroyasu model during the whole injection process.

The perturbation plot is employed as a comparison among the effects of all factors at a certain point (usually the midpoint) under all conditions. In the perturbation plots, the responses are plotted by varying one factor and fix others. Therefore, a steep slope of a factor means the response is sensitive to it, whilst a flat line indicates insensitivity.

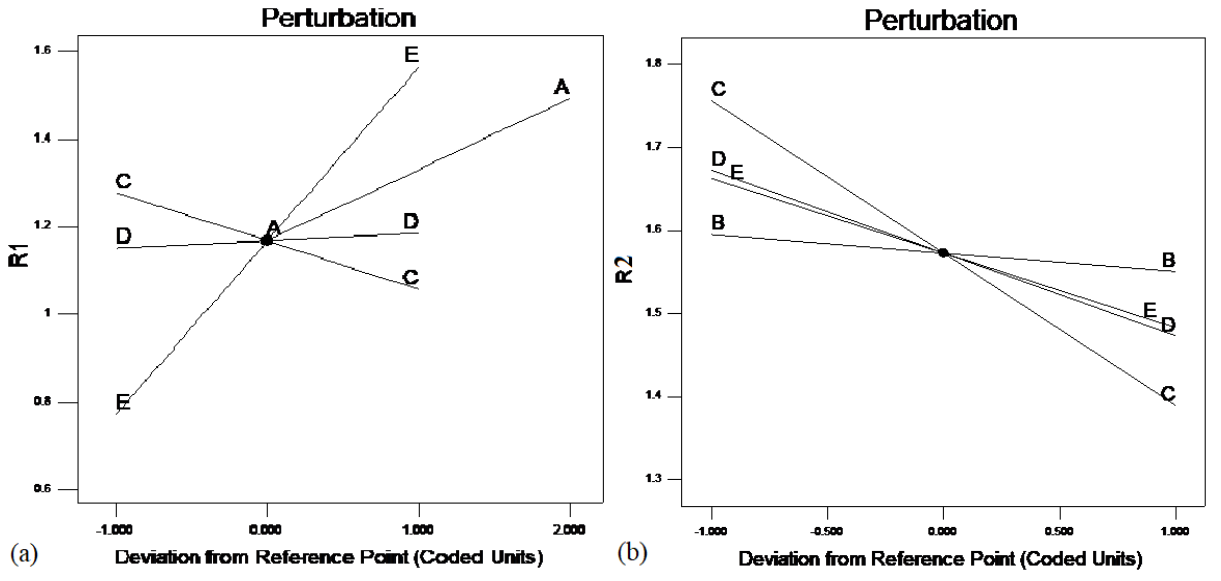

Fig. 15. Perturbation plots of the R1 (a) and R2 (b) models

As shown in **Fig. 15**, the spray tip penetration before the EOI is easily impacted by rail pressure and sample time, but that after the EOI is most sensitive to the ambient pressure, which is also inconsistency with the results in Fig. 8 ~ Fig.11.

7. Conclusions

In this paper, a CFD model is established to investigate the independent and interactive impacts of fuel temperature, rail pressure, ambient temperature and ambient pressure on the macroscopic characteristics of HVO, with the spray experiment conducted in a CVV system. Furthermore, the correlations between these variables and spray tip penetrations during injection and post-injection periods are obtained. The main conclusions are drawn as follows

- The Wave model is better than KHRT model and it can predict the spray tip penetration and average cone angle well compared with the experimental data.

- The average cone angle becomes larger at high ambient pressure, and the impact of ambient pressure can be weakened by increasing ambient temperature at 600 bar rail pressure but improved at a high ambient temperature and 1800 bar rail pressure.
- During the injection period, the spray tip penetration can be significantly promoted by higher rail pressure and lower ambient pressure at all conditions due to the promotion to droplets breakup. The ambient temperature and fuel temperature only have small influence.
- During the post-injection period (after the EOI), penetrations at most conditions significantly decrease when increasing ambient temperature and fuel temperature because evaporation dominates this period.
- Two DoE models are formulated to predict spray tip penetrations before and after the EOI. Moreover, the rail pressure, ambient pressure and sample time are all significant factors in the two models, whilst ambient temperature is only significant for the post-injection model.

Acknowledgements

The authors would like to thank the supports by EPSRC through (EP/K503885/1) for the project Study of engine waste heat technologies, from NSFC-RS Joint Project under the grant number No. 5151101443 and IE/151256.The first author also would like to thank for sponsorship towards the PhD study from the SAgE doctoral Training Award under grant number NH/140671210 and financial support from Chinese Scholarship Council under No. 201508060054. The support from Cao Guang Biao High Tech Talent Fund, Zhejiang University are also highly acknowledged.

References

[1] F. Millo, B.K. Debnath, T. Vlachos, C. Ciaravino, L. Postrioti, G. Buitoni, Effects of different biofuels blends on performance and emissions of an automotive diesel engine, Fuel, 159 (2015) 614-627.

[2] T. Bohl, A. Smallbone, G. Tian, A.P. Roskilly, Particulate number and NOx trade-off comparisons between HVO and mineral diesel in HD applications, Fuel, 215 (2018) 90-101.

[3] G. Labeckas, S. Slavinskas, I. Kanapkienė, The individual effects of cetane number, oxygen content or fuel properties on performance efficiency, exhaust smoke and emissions of a

turbocharged CRDI diesel engine–Part 2, Energy Conversion and Management, 149 (2017) 442-466.
[4] H. Aatola, M. Larmi, T. Sarjovaara, S. Mikkonen, Hydrotreated vegetable oil (HVO) as a renewable diesel fuel: trade-off between NOx, particulate emission, and fuel consumption of a heavy duty engine, SAE International Journal of Engines, 1 (2008) 1251-1262.
[5] S.-Y. No, Application of hydrotreated vegetable oil from triglyceride based biomass to CI engines–A review, Fuel, 115 (2014) 88-96.
[6] K. Sugiyama, I. Goto, K. Kitano, K. Mogi, M. Honkanen, Effects of hydrotreated vegetable oil (HVO) as renewable diesel fuel on combustion and exhaust emissions in diesel engine, SAE International Journal of Fuels and Lubricants, 5 (2012) 205-217.
[7] K. Lehto, A. Elonheimo, K. Hakkinen, T. Sarjovaara, M. Larmi, Emission reduction using hydrotreated vegetable oil (HVO) with Miller timing and EGR in diesel combustion, SAE International Journal of Fuels and Lubricants, 5 (2011) 218-224.
[8] D. Singh, K. Subramanian, S. Singal, Emissions and fuel consumption characteristics of a heavy duty diesel engine fueled with hydroprocessed renewable diesel and biodiesel, Applied Energy, 155 (2015) 440-446.
[9] P.-C. Chen, W.-C. Wang, W.L. Roberts, T. Fang, Spray and atomization of diesel fuel and its alternatives from a single-hole injector using a common rail fuel injection system, Fuel, 103 (2013) 850-861.
[10] B. Mohan, W. Yang, K.L. Tay, W. Yu, Experimental study of spray characteristics of biodiesel derived from waste cooking oil, Energy Conversion and Management, 88 (2014) 622-632.
[11] Y. Gao, M. Wei, F. Yan, L. Chen, G. Li, L. Feng, Effects of cavitation flow and stagnant bubbles on the initial temporal evolution of diesel spray, Experimental Thermal & Fluid Science, 87 (2017).
[12] Y. Ma, R. Huang, S. Huang, Y. Zhang, S. Xu, Z. Wang, Experimental investigation on the effect of n-pentanol blending on spray, ignition and combustion characteristics of waste cooking oil biodiesel, Energy Conversion and Management, 148 (2017) 440-455.
[13] Y. Ma, S. Huang, R. Huang, Y. Zhang, S. Xu, Spray and evaporation characteristics of n-pentanol–diesel blends in a constant volume chamber, Energy Conversion and Management, 130 (2016) 240-251.
[14] E. Mancaruso, L. Sequino, B.M. Vaglieco, Analysis of spray injection in a light duty CR diesel engine supported by non-conventional measurements, Fuel, 158 (2015) 512-522.
[15] T. Hulkkonen, H. Hillamo, T. Sarjovaara, M. Larmi, Experimental study of spray characteristics between hydrotreated vegetable oil (HVO) and crude oil based EN 590 diesel fuel, in, SAE Technical Paper, 2011, pp. 24-0042.
[16] T. Bohl, G. Tian, A. Smallbone, A.P. Roskilly, Macroscopic spray characteristics of next-generation bio-derived diesel fuels in comparison to mineral diesel, Applied Energy, 186 (2017) 562-573.
[17] H.M. Ismail, H.K. Ng, S. Gan, Evaluation of non-premixed combustion and fuel spray models for in-cylinder diesel engine simulation, Applied Energy, 90 (2012) 271-279.
[18] V.G. Levich, Physicochemical hydrodynamics, Prentice hall, 1962.
[19] M. Battistoni, C.N. Grimaldi, Numerical analysis of injector flow and spray characteristics from diesel injectors using fossil and biodiesel fuels, Applied Energy, 97 (2012) 656-666.

[20] T. Kim, S. Park, Modeling flash boiling breakup phenomena of fuel spray from multi-hole type direct-injection spark-ignition injector for various fuel components, Energy Conversion and Management, 160 (2018) 165-175.
[21] M.H. Azami, M. Savill, Modelling of spray evaporation and penetration for alternative fuels, Fuel, 180 (2016) 514-520.
[22] B. Vajda, L. Lešnik, G. Bombek, I. Biluš, Z. Žunič, L. Škerget, M. Hočevar, B. Širok, B. Kegl, The numerical simulation of biofuels spray, Fuel, 144 (2015) 71-79.
[23] Y. Gong, O. Kaario, A. Tilli, M. Larmi, F. Tanner, A computational investigation of hydrotreated vegetable oil sprays using RANS and a modified version of the RNG k-ε model in OpenFOAM, in, SAE Technical Paper, 2010, pp. 01-0739.
[24] J.D. Naber, D.L. Siebers, Effects of gas density and vaporization on penetration and dispersion of diesel sprays, in, SAE technical paper, 1996.
[25] H. Hiroyasu, T. Kadota, M. Arai, Supplementary comments: fuel spray characterization in diesel engines, Combustion modeling in reciprocating engines, 369 (1980).
[26] L. Chen, L. Feng, Z. Liu, G. Li, Y. Li, Y. Lu, A.P. Roskilly, L. Chen, L. Feng, Z. Liu, Quantifying the effects of fuel compositions and process variables on planar surface area and spray non-uniformity via combined mixture-process design of experiment, Atomization & Sprays, 27 (2017) 707-722.
[27] L. Chen, Z. Zhang, W. Gong, Z. Liang, Quantifying the effects of fuel compositions on GDI-derived particle emissions using the optimal mixture design of experiments, Fuel, 154 (2015) 252-260.
[28] L. Chen, Z. Liu, P. Sun, W. Huo, Formulation of a fuel spray SMD model at atmospheric pressure using Design of Experiments (DoE), Fuel, 153 (2015) 355-360.
[29] A.B. Liu, D. Mather, R.D. Reitz, Modeling the effects of drop drag and breakup on fuel sprays, in, DTIC Document, 1993.
[30] R. REITZ, Modeling atomization processes in high-pressure vaporizing sprays, Atomisation and Spray Technology, 3 (1987) 309-337.
[31] W. Waidmann, A. Boemer, M. Braun, Adjustment and verification of model parameters for diesel injection CFD simulation, in, SAE Technical Paper, 2006, pp. 01-0241.
[32] J. Legg, A. Narvaez, V. McDonell, Performance of algae-derived renewable diesel in a twin-fluid airblast atomizer, in: Proceedings of the 12th triennial international conference on liquid atomization and spray systems, Heidelberg, Germany Google Scholar, 2012, pp. 56-65.
[33] C.T.S. Turk, U.C. Oz, T.M. Serim, C. Hascicek, Formulation and optimization of nonionic surfactants emulsified nimesulide-loaded PLGA-based nanoparticles by design of experiments, AAPS PharmSciTech, 15 (2014) 161-176.